Published OnlineFirst September 26, 2014; DOI: 10.1158/0008-5472.CAN-14-1106

Therapeutics, Targets, and Chemical Biology

Cancer Research

Targeting Cancer Stem–like Cells as an Approach to Defeating Cellular Heterogeneity in Ewing Sarcoma

Sandrine Cornaz-Buros[1], Nicolo Riggi[2], Claudio DeVito[3], Alexandre Sarre[4], Igor Letovanec[5], Paolo Provero[6], and Ivan Stamenkovic[1]

Abstract

Plasticity in cancer stem–like cells (CSC) may provide a key basis for cancer heterogeneity and therapeutic response. In this study, we assessed the effect of combining a drug that abrogates CSC properties with standard-of-care therapy in a Ewing sarcoma family tumor (ESFT). Emergence of CSC in this setting has been shown to arise from a defect in TARBP2-dependent microRNA maturation, which can be corrected by exposure to the fluoroquinolone enoxacin. In the present work, primary ESFT from four patients containing $CD133^+$ CSC subpopulations ranging from 3% to 17% of total tumor cells were subjected to treatment with enoxacin, doxorubicin, or both drugs. Primary ESFT CSC and bulk tumor cells displayed divergent responses to standard-of-care chemotherapy and enoxacin. Doxorubicin, which targets the tumor bulk, displayed toxicity toward primary adherent ESFT cells in culture but not to CSC-enriched ESFT spheres. Conversely, enoxacin, which enhances miRNA maturation by stimulating TARBP2 function, induced apoptosis but only in ESFT spheres. In combination, the two drugs markedly depleted CSCs and strongly reduced primary ESFTs in xenograft assays. Our results identify a potentially attractive therapeutic strategy for ESFT that combines mechanism-based targeting of CSC using a low-toxicity antibiotic with a standard-of-care cytotoxic drug, offering immediate applications for clinical evaluation. *Cancer Res; 74(22); 6610–22. ©2014 AACR.*

Introduction

Tumor cell plasticity and heterogeneity may actively shape response to conventional chemotherapy in solid malignancies and underlie relapse following seemingly successful treatment. Heterogeneity among tumor cells within the same tumor mass may arise by numerous nonmutually exclusive mechanisms. They include stochastic genetic (1) and epigenetic (2) changes that cause intrinsic differences among cancer cells, leading to clonal selection; microenvironmental cues that induce phenotypic and functional differences among cancer cells in different locations (3); and hierarchical organization of tumor cells, where a small, poorly differentiated cell subpopulation with self-renewing and tumor-initiating properties gives rise to more differentiated cells, most of which have lost tumorigenicity (4). Cells that occupy the apex of such hierarchies are currently referred to as cancer stem cells (CSC). Whereas the existence and properties of CSC have been well established in certain leukemias (5), they have been somewhat more challenging to define in solid malignancies, partly because of the lack of robust cell surface markers and partly because lineage tracing in epithelial and mesenchymal tumors is less well defined than in hematopoietic malignancies. Nevertheless, there is growing evidence to support the existence of CSC in solid tumors of diverse ontogeny and histotypes (6, 7).

In addition to providing a driving force for tumor growth and maintenance, CSC may display different sensitivity to cytotoxic drugs and radiotherapy than the bulk tumor cell population that they generate (8–10). Thus, in at least some tumor types, CSC may withstand conventional anticancer therapy consistent with their presumed role in relapse following therapy, while possibly responding to approaches that impair pluripotency. Attempts to augment therapeutic effectiveness in tumors with a documented cellular hierarchy should therefore include strategies that target not only rapidly dividing bulk and progenitor cells, but CSC plasticity as well.

Ewing sarcoma family tumors (ESFT), the second most frequent bone malignancy in children and young adults (11), are among the few sarcoma types in which CSCs have been identified and characterized (12). ESFT pathogenesis is dictated by a chromosomal translocation that creates a fusion between sequences encoding the EWSR1 transactivation domain and those encoding the DNA-binding domain of one of several possible ets transcription factor family members. In

[1]Experimental Pathology Service, CHUV and University of Lausanne, Lausanne, Switzerland. [2]Department of Pathology, Massachusetts General Hospital, Harvard Medical School, Boston, Massachusetts. [3]Department of Pathology, HUG and University of Geneva, Geneva, Switzerland. [4]Mouse Cardiovascular Assessment Facility, University of Lausanne, Lausanne, Switzerland. [5]Clinical Pathology Service, CHUV and University of Lausanne, Lausanne, Switzerland. [6]Center for Translational Genomics and Bioinformatics, San Raffaele Scientific Institute, Milan, Italy.

Note: Supplementary data for this article are available at Cancer Research Online (http://cancerres.aacrjournals.org/).

S. Cornaz-Buros and N. Riggi contributed equally to this article.

Corresponding Author: Ivan Stamenkovic, Institute of Pathology, 25 Rue du Bugnon, CH-1011 Lausanne, Switzerland. E-mail: Ivan.Stamenkovic@chuv.ch

doi: 10.1158/0008-5472.CAN-14-1106

Published OnlineFirst September 26, 2014; DOI: 10.1158/0008-5472.CAN-14-1106

85% of ESFT cases, the EWSR1 fusion partner is FLI-1, resulting from the chromosomal translocation t(11;22)(q24;q12) (13). The *EWS-FLI1* fusion gene encodes an aberrant transcription factor, which, in a permissive cellular context, triggers transcriptional reprogramming that culminates in target cell transformation.

Primary ESFT harbor a subpopulation of cells that express CD133, a hematopoietic stem-cell marker associated with, but not specific for, CSCs in a variety of solid tumors (12). These cells constitute 3% to 15% of most primary ESFT and display plasticity, clonogenicity, tumor-initiating capacity, and the ability to generate nontumorigenic progeny, all of which are consistent with CSC features. Moreover, primary ESFT cells retain CSC properties when cultured as spheres under low attachment conditions in serum-free knockout (KO) medium but lose them in serum-supplemented monolayer culture (14). We recently discovered that ESFT CSC display partial and reversible repression of TARBP2, which participates in maturation of small noncoding RNAs (microRNAs, miRNAs), resulting in a defective miRNA repertoire (14). By binding to the complementary sequences in multiple different transcripts, miRNAs can modulate the expression of entire gene networks (15), and miRNA implication in the pathogenesis of diverse cancers is well established (16). Defective TARBP2-dependent miRNA maturation causes downregulation of a broad miRNA repertoire that contributes to the emergence of CSC in ESFT (17), whereas restoration of its expression by introduction of exogenous TARBP2 abrogates CSC properties (14). Enhancement of TARBP2 function may, therefore, provide an attractive therapeutic strategy toward eliminating CSCs in ESFT.

Their poor prognosis despite aggressive multimodal therapy (11), dependence on EWS-FLI-1 expression as the sole oncogenic event in the majority of cases (18), and possession of an identified mechanism that underlies the emergence of their CSC subpopulation render ESFT an ideal candidate malignancy to address the effect of combining conventional standard-of-care chemotherapy with selective CSC targeting. Enoxacin, a fluoroquinolone family antibiotic used for treatment of urinary tract infections, increases TARBP2 binding affinity for its precursor miRNAs in mammalian cells, resulting in the enhancement of miRNA maturation (19). Accordingly, we have shown that enoxacin can impair ESFT CSC properties *in vitro* by restoring their miRNA repertoire (14). Here, we assessed the effect of enoxacin alone or in combination with standard-of-care therapy on primary ESFT xenografts *in vivo* in an effort to define a clinically relevant therapeutic strategy that targets both CSCs and the tumor bulk. We show that such an approach has a potent inhibitory effect on ESFT growth *in vivo* and that it may provide an attractive therapeutic option.

Materials and Methods

Cell culture

A673 (ATCC) and TC252 (kindly provided by Dr. T. Triche, Childrens Hospital Los Angeles, University of Southern California, Los Angeles, CA) ESFT cells lines were cultured in RPMI (Gibco) supplemented with 10% FCS (Gibco). Primary ESFT samples were obtained at surgery with the approval of the ethics committee of the Canton de Vaud. All human samples were anonymized before analysis and were exempted from informed consent in accordance with the law of the Canton de Vaud. Spheres were cultured in IMDM (Gibco), supplemented with 20% KO serum (Gibco), 10 mg/mL LIF (Millipore), 10 ng/mL recombinant human EGF (Invitrogen), and 10 ng/mL recombinant human bFGF (Invitrogen) in ultra-low attachment flasks (Corning). Adherent cells were derived from spheres by culture in IMDM (Gibco) supplemented with 10% FCS (Gibco). Human pediatric mesenchymal stem cells (hpMSC) were isolated and cultured as described (17). shRNA depletion of TARBP2 was performed as described (14).

RNA isolation and real-time PCR

Total RNA was isolated using Trifast (Peqlab) as recommended. Real-time PCR was performed as previously described (17). TaqMan probes included 18S, *OCT4*, and *NANOG* (Applied Biosystems). Primer sequences for *ONECUT2* SYBR Green gene expression quantification were: forward, 5′-CTCTTTGCGTTTGCACGCTG-3′; reverse, 5′-GGAATCCAAAACCGTGGAGTAA-3′. For microRNA quantification, 30 ng of total RNA was amplified using the miRCURY LNA Universal RT microRNA PCR Kit (Exiqon) according to the manufacturer's recommendations. LNA PCR primers (Exiqon) were used for RT-PCR amplification, and snord49a provided the endogenous control.

Cell growth, apoptosis, Western blot, and FACS analysis

ESFT cell lines were plated in triplicate wells and total cell counts and cell viability were determined using Trypan Blue. MTS assays were performed according to standard procedures (CellTiter 96; Promega). FACS analysis using anti-CD133 antibody (Miltenyi) was performed as previously described (12). Cells (sphere/adherent/cell lines) were harvested with their medium and apoptosis assays were performed using the FITC Annexin V Apoptosis Detection Kit I (BD Biosciences) as recommended. Western blot analyses were performed according to standard procedures, with anti-TARBP2 antibody from Abnova (#MAB0811).

Clonogenic and tumorigenicity assays

Single primary ESFT cells were suspended in four 96-well plates and cultured for 30 days in IMDM, 20% KO serum, supplemented with LIF, EGF, and FGF and treated with DMSO or 40 μg/mL enoxacin. Spheres were scored 15 days later. Five thousand sphere-derived or adherent ESFT cells were injected beneath the renal capsule of 18 NSG mice each. All mice were sacrificed 3 months later and kidneys subjected to histologic analysis.

Mouse treatment, tumor monitoring, and statistical analysis

Experimental protocols involving mice were approved by the Veterinary Service of the Canton of Vaud (Etat de Vaud, Service Vétérinaire), under authorization number VD2488. NSG mice (2 × 28) were anesthetized and 10,000 sphere-derived cells from ESFT-3 and 5,000 sphere-derived ESFT-1 cells were injected beneath the renal capsule and allowed to engraft for 10 days. DMSO (10%) or enoxacin 50 mg/kg in 10% DMSO was then administered i.p. with or without doxorubicin,

Published OnlineFirst September 26, 2014; DOI: 10.1158/0008-5472.CAN-14-1106

0.5 mg/kg weekly. Tumor growth was monitored by ultrasound imaging using a 40-MHz probe and the Vevo 2100 Ultrasound machine (VisualSonics). Tumor volume was calculated by $V = 4/3\ p(Dd \times Ds \times Dt)/8$, where Dd corresponds to tumor height, and Ds and Dt to tumor lengths measured in long- and short-axis views, respectively. When control tumors reached 1 cm^3, mice were sacrificed. Tumors were then harvested and processed for RNA extraction, H&E staining, IHC and, when possible, 200 mg of tumor tissue was enzymatically dissociated for single-cell CD133 FACS analysis. Five thousand cells from treated tumors were reinjected into new recipient NGS mice and left to grow for 6 to 8 weeks. All statistical analyses were performed using GraphPad Prism 6.

Results

Characterization of the ESFT CSC model *in vitro* and *in vivo*

ESFTs from four patients were obtained at surgery. ESFT-1, ESFT-2, ESFT-3, and ESFT-4 expressed variant 1 of the EWS-FLI-1 fusion protein and were, respectively, a retroperitoneal tumor removed immediately following chemotherapy, an untreated vertebral tumor, a metastatic lesion to the lung following relapse and failure of multiple rounds of chemotherapy, and a tumor that had relapsed 7 years following cessation of treatment. Freshly removed cells from each of the four tumors were assessed for CD133 expression, sphere-forming ability *in vitro*, and tumorigenic potential *in vivo*. $CD133^+$ cells represented 5.7% and 10.1% of the total tumor cell population of ESFT-1 and -4, respectively, (Supplementary Fig. S1A), whereas the starting material of ESFT-2 and -3 was insufficient to allow for FACS analysis. Cells from all four tumors formed spheres under appropriate culture conditions and the $CD133^+$ population within cultured spheres ranged from 2.7% to 40%. The $CD133^-$ bulk of the tumor cells did not possess sphero-genic properties. After 2 to 3 weeks of culture in serum-free medium, $CD133^+$ cell-derived spheres were disaggregated and half of the cells were reseeded in suspension in serum free, growth factor–supplemented knockout (KO) medium (14), whereas the other half were plated as adherent monolayers in serum-supplemented medium. Thus, all subsequent comparisons for response to treatment *in vitro* were made on cells derived from the same initial population.

Upon injection of 5,000 cells into the subcapsular renal compartment of NOD/SCID/c-γKO (NSG) mice, all sphere-derived cells formed tumors that phenocopied the original growth (data not shown). In contrast, the same number of adherent cells from three (ESFT-1, -2, and -4) tumors did not display tumor-initiating capacity, whereas adherent ESFT-3 cells formed tumors that grew more slowly than their sphere-derived counterparts (Supplementary Fig. S1B). It is possible that metastasis-derived cells, which had survived numerous rounds of chemotherapy, incurred genetic events that were not epigenetically erased by *in vitro* culture and that may confer tumor-initiating capacity to a broader cell subpopulation, reducing cellular hierarchy (18).

Consistent with our earlier observations that ESFT $CD-133^+$ sphere-forming cells display defective maturation of miRNAs, including regulators of core reprogramming gene expression (14), *NANOG* and *OCT4* transcripts were significantly higher in spheres than in adherent cells from all four tumors, the greatest difference residing in ESFT-2 cells derived from an untreated tumor (Fig. 1A). ESFT-3–adherent cells, which retained tumor-initiating capacity, had *NANOG* and *OCT4* expression levels closer to those of the corresponding spheres than their ESFT-1, -2, and -4 counterparts (Fig. 1A). A subset of TARBP2-dependent miRNAs whose repression is implicated in ESFT tumorigenesis was downregulated in spheres from all three tumor samples (Fig. 1B), consistent with a reversible defect in miRNA maturation in KO-cultured tumorigenic cells, as previously suggested (14).

ESFT spheres and adherent cells display reciprocal sensitivity to doxorubicin and enoxacin *in vitro*

Because chemoresistance is one of the suggested CSC properties in at least some tumor types (20), we compared sensitivity to doxorubicin, a first-line cytotoxic drug in ESFT (11), of primary ESFT cells grown as spheres and as adherent monolayers. Cells were treated with single 10-fold incremental doses of doxorubicin (within a concentration range of 17.2 to 1,720 nmol/L) for 96 hours in culture and assessed for proliferation by an MTS assay, normalized to that of DMSO-treated cells. All four tumor-derived adherent cell cultures were significantly more prone to growth inhibition by doxorubicin than their sphere counterparts at all concentrations tested (Fig. 2A).

On the basis of our earlier demonstration that enoxacin inhibits growth of ESFT cell lines *in vitro*, we explored the effect of the drug on primary ESFT. Dose–response analysis within a range of 5 to 80 μg/mL revealed significant inhibition of ESFT-1 sphere growth at 10 μg/mL with a near maximal effect at 40 μg/mL (data not shown). We therefore subjected the four tumor-derived cell batches to enoxacin at a dose of 10 μg/mL, which corresponds to plasma concentrations of the drug administered to patients with urinary tract infection (21), and observed significant growth inhibition of spheres from all four ESFTs (Fig. 2B). Enoxacin had a minor effect on TC 252 ESFT cells, but no effect on either A673 ESFT cells or primary hpMSCs, from which ESFT are believed to originate (Fig. 2B; ref. 17). Importantly, enoxacin had a distinct effect on ESFT spheres and adherent cells, with virtually no inhibition of adherent ESFT-2, -3, and -4 cell growth (Fig. 2C). To further interrogate the role of TARBP2 repression in ESFT cell sensitivity to enoxacin, proliferation of A673 cells depleted of TARBP2 by targeted shRNA expression was assessed in response to 10 μg/mL of enoxacin. As expected, inhibition of proliferation was markedly stronger in TARBP2-depleted than in control A673 cells after 48 and 72 hours of treatment (Fig. 2D).

Enoxacin induces $CD133^+$ cell death and abrogates ESFT self-renewal *in vitro*

Having shown that ESFT spheres display sensitivity to enoxacin at low doses, we addressed the selectivity of the effect of enoxacin for CSCs by examining $CD133^+$ cell viability (Fig. 3A, left) following *in vitro* treatment with enoxacin at 40 μg/mL (the dose previously applied to ESFT cells; ref. 14). Cells were colabeled with Annexin, PI, and anti-CD133 antibody and

Published OnlineFirst September 26, 2014; DOI: 10.1158/0008-5472.CAN-14-1106

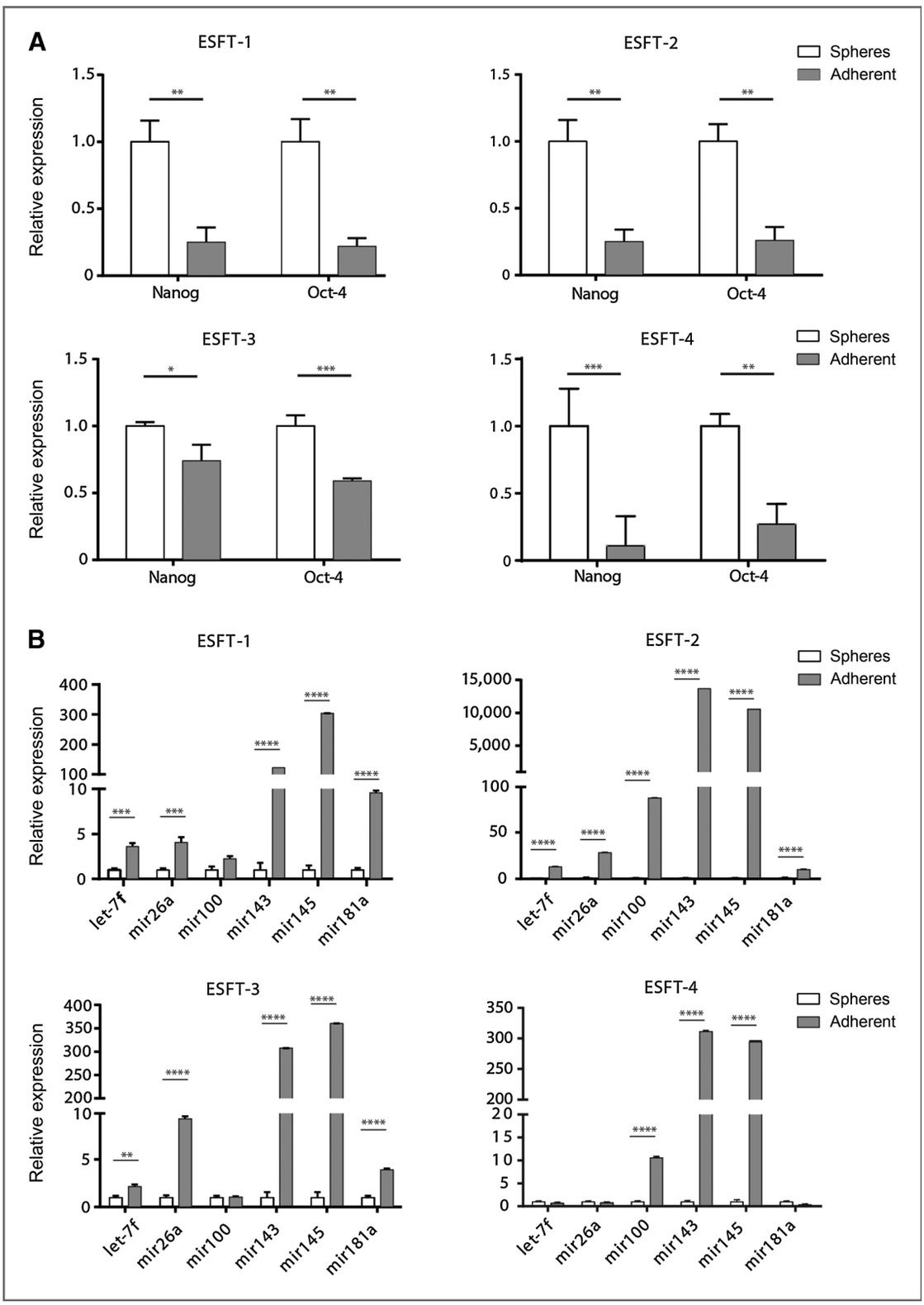

Figure 1. miRNA and pluripotency gene expression profiles in primary ESFT spheres and adherent cells *in vitro*. A, expression of *NANOG* and *OCT-4*, as measured by RT-PCR, expressed as fold changes in spheres and adherent cells from the four primary ESFT. B, fold change of expression of selected miRNAs as measured by RT-PCR in the same spheres and adherent cells as in A. Results were analyzed by one-way ANOVA, and mean values with SD are shown. *, $P < 0.05$; **, $P < 0.01$; ***, $P < 0.001$; ****, $P < 0.0001$.

Published OnlineFirst September 26, 2014; DOI: 10.1158/0008-5472.CAN-14-1106

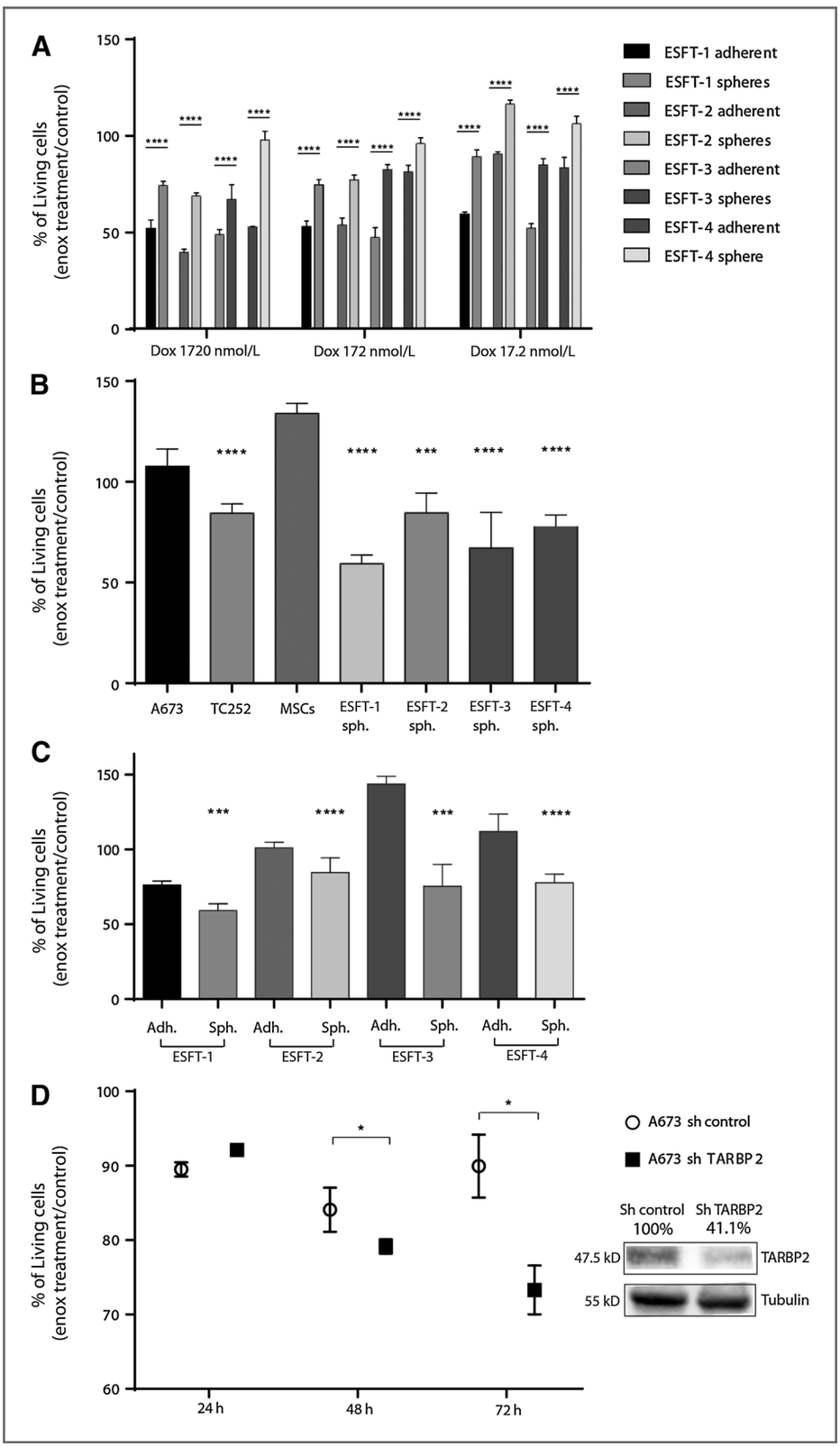

Figure 2. Differential response to doxorubicin and enoxacin of CSC-enriched primary ESFT spheres, adherent cells, and cell lines. Effect of 96-hour primary sphere and adherent cell treatment with increasing doses of doxorubicin as assessed by MTS. A, proportion of living cells relative to control treated cells. Data were analyzed by two-way ANOVA. B and C, effect on spheres, adherent cells, and cell lines of 96-hour 10 μg/mL enoxacin treatment as assessed by MTS. The proportion of living cells relative to control-treated cells is shown (B, tumor cell line and hpMSC compared with primary sphere response; C, primary sphere compared to corresponding adherent cell response). D, left, ratio of living cells to control-treated cells after 24, 48, and 72 hours of 10 μg/mL of enoxacin treatment of sh control or shTARBP2-infected A673 cells. D, right, Western blotting and TARBP2 quantification in A673 cells bearing sh control or shTARBP2. Results from growth curves analyzed by two-way ANOVA and significance of enoxacin-treated relative to control-treated cells are shown. *, $P < 0.05$; ***, $P < 0.001$; ****, $P < 0.0001$.

Published OnlineFirst September 26, 2014; DOI: 10.1158/0008-5472.CAN-14-1106

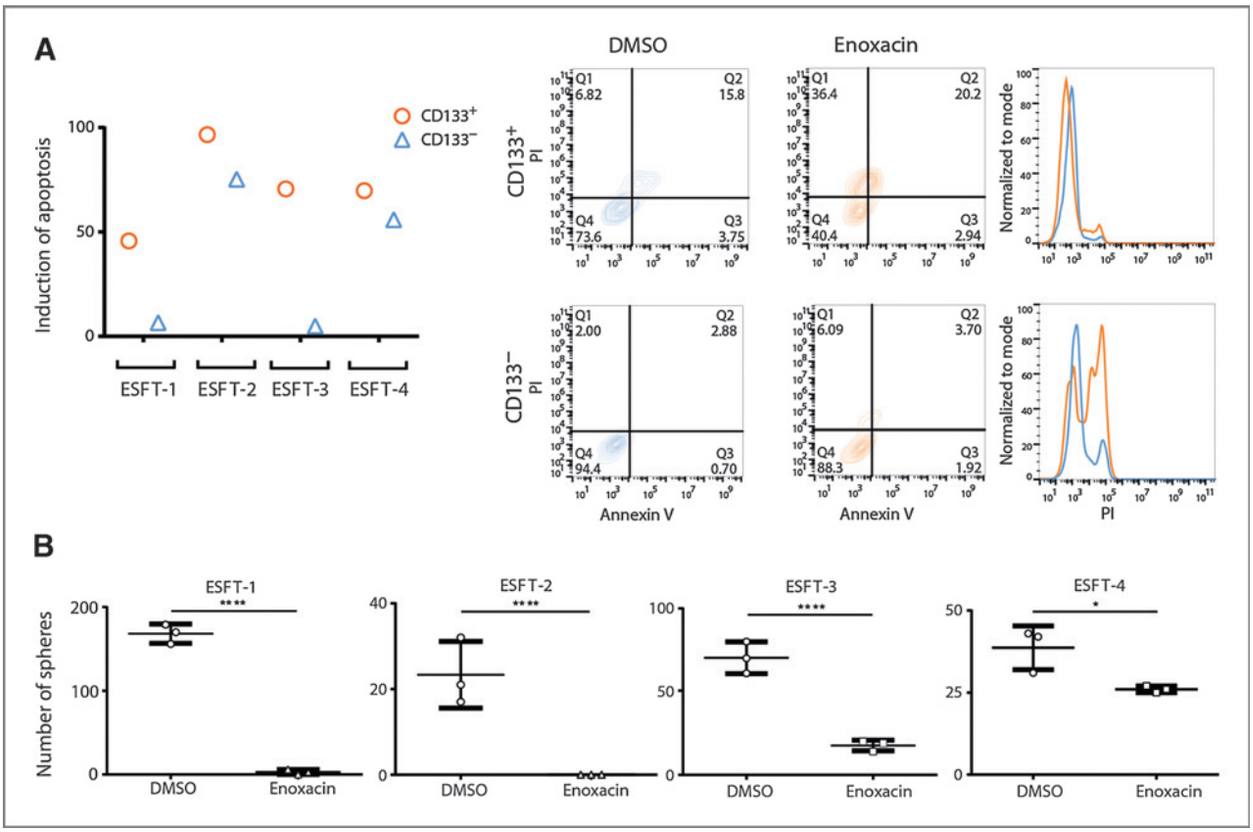

Figure 3. Induction of apoptosis selectively in CD133$^+$ cells by enoxacin. A, induction of apoptosis in enoxacin-treated relative to control-treated CD133$^+$ and CD133$^-$ cells, as measured by Annexin PI staining of cells harvested at subconfluence. Dots and triangles, induction of apoptosis in CD133$^+$ and CD133$^-$ populations, respectively, from the four tumors as indicated (left). FACS image of Annexin V and PI staining of ESFT-1 cells gated on the CD133$^+$ and CD133$^-$ subpopulations (right). Graphs are representative of three independent experiments. B, sphere formation by DMSO- and enoxacin-treated cells. Graphs, sphere number. Data were analyzed by the Student *t* test. Mean values ± SD are shown. *, $P < 0.05$; ****, $P < 0.0001$.

gating adjusted to either the CD133$^+$ or the CD133-population (Fig. 3A, right and Supplementary Fig. S2). CD133$^+$ cells from all four tumors displayed significant to near total (ESFT-2) induction of apoptosis in response to treatment (Fig. 3A, left). CD133$^-$ cells from ESFT-1 and -3 were resistant to enoxacin (Fig. 3A, left), whereas ESFT-2 and -4 CD133$^-$ cells displayed sensitivity that was closer to that of the corresponding CD133$^+$ cells.

Because enoxacin induced apoptosis in 50% to nearly 100% of the ESFT CD133$^+$ cells *in vitro*, we assessed whether depletion of these cells corresponds to loss of self-renewal by plating a single ESFT cell per well in a 96-well plate and adding DMSO or enoxacin to the culture medium. After 2 weeks, almost no spheres formed in enoxacin-supplemented ESFT-1 and ESFT-2 cultures (Fig. 3B). Some spheres were still formed by ESFT-3 and ESFT-4 cells, which were derived from a tumor that had become resistant to all conventional treatment regimens and a tumor that had relapsed 7 years following cessation of treatment, respectively.

Enoxacin alone has a moderate impact on the growth of primary ESFT xenografts

Slow growth of ESFT-2 and -4 xenotransplants precluded their use in treatment assays *in vivo*, leaving us to focus on ESFT-1 and ESFT-3. To assess the effect of enoxacin treatment *in vivo*, 5,000 ESFT-1 cells and 10,000 ESFT-3 cells were injected into the subcapsular renal compartment of NSG mice and allowed to engraft for 10 days. Two groups of six mice each were administered either DMSO or enoxacin (50 mg/kg i.p. daily 5 days a week, which corresponds to a slightly higher dose than that used for urinary tract infections in humans; ref. 21), and the response was monitored by ultrasound imaging until control tumors reached a volume of 1 cm^3. Animals were then sacrificed and tumors processed for histologic analysis. Consistent with its targeting of a small subpopulation of cells, enoxacin had a limited effect on tumor weight (Fig. 4A, left). However, enoxacin-treated tumors displayed a distinct consistency and gross appearance compared with control tumors that reflected partial tissue disaggregation and multifocal necrosis (Fig. 4B). Assessment of CD133 expression in residual tumor cells revealed that the treatment had almost completely depleted the CD133$^+$ subpopulation in ESFT-1 (Fig. 4A, right). A similar trend was observed in ESFT-3 xenotransplants albeit with greater variability (Fig. 4A, right). Both xenografts were composed of typical ESFT small round cells and expressed CD99 as assessed by immunohistochemistry (Fig. 4C).

Published OnlineFirst September 26, 2014; DOI: 10.1158/0008-5472.CAN-14-1106

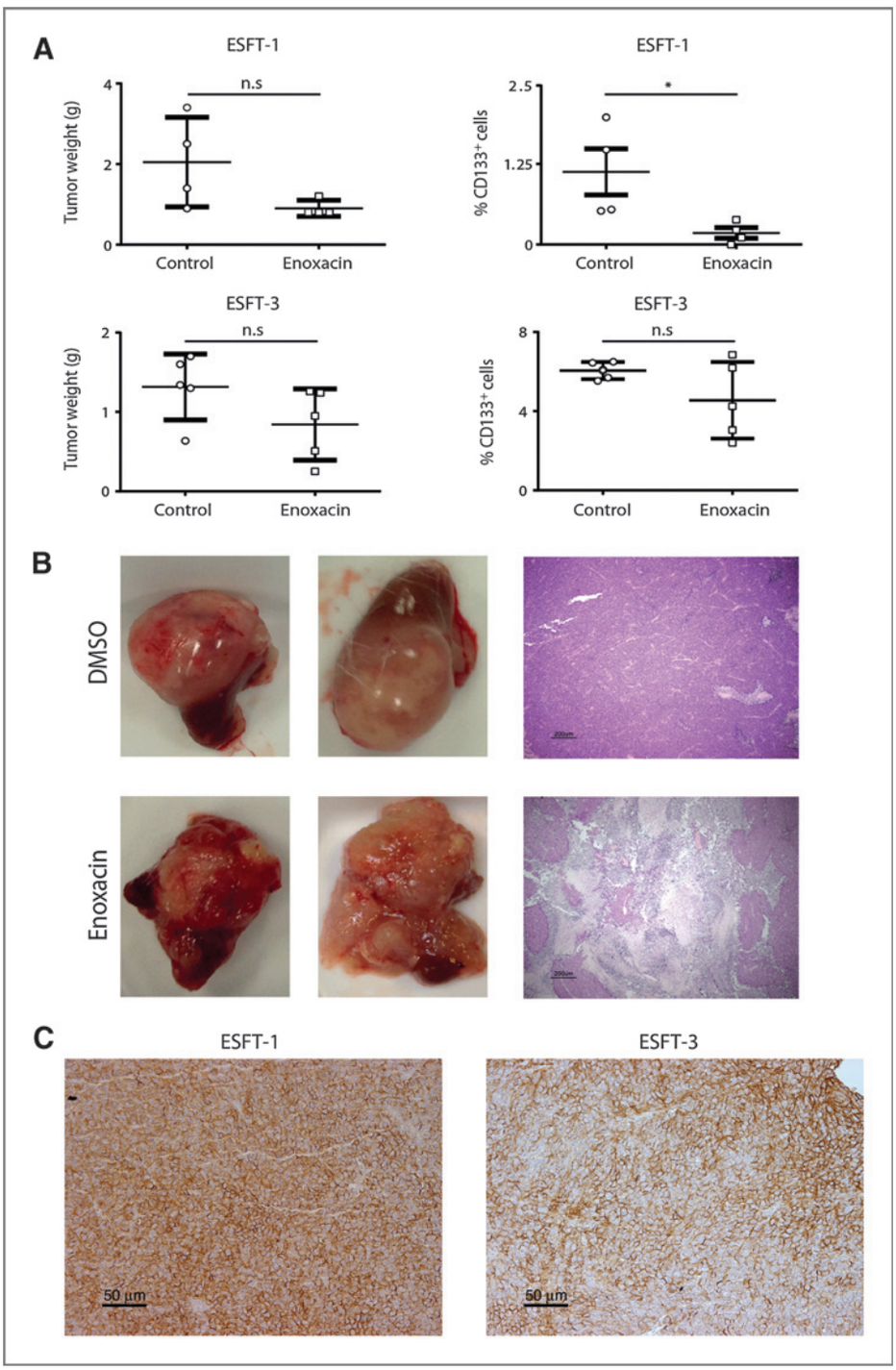

Figure 4. Enoxacin alone depletes the CD133$^+$ compartment but is not sufficient to inhibit primary ESFT xenograft growth. 5,000 ESFT-1 and 10,000 ESFT-3 cells were injected into the subcapsular kidney compartment of NGS mice and treatment was started 10 days later. A, left, tumor weight after 5 weeks of 5 day/week treatment with vehicle or 50 mg/kg of enoxacin alone; right, CD133$^+$ subpopulation fractions in residual tumors at the end of the 5-week treatment. The Student *t* test was performed on the two groups. n.s., nonsignificant. B, gross anatomy and histology of two representative control- and enoxacin-treated ESFT-3. C, CD99 staining of ESFT 1 and ESFT-3 xenografts. *, $P < 0.05$.

The combination of enoxacin and doxorubicin efficiently inhibits ESFT growth *in vivo*

Evidence suggesting that nontumorigenic cancer cells may undergo reprogramming toward CSCs (6) supports the need for simultaneous targeting of both cell subpopulations. We therefore assessed the effect of combining treatment targeting CSCs with treatment directed at the tumor bulk. Using the same primary ESFT xenograft model as above, we added doxorubicin to the treatment regimen at a single weekly dose of 0.5 mg/kg. Enoxacin or DMSO was administered daily for 5 days/week until DMSO-treated tumors reached a size of 1 cm^3. Ultrasound assessment of tumor growth revealed distinct responses to the different regimens (Fig. 5A), that were comparable among the different tumors examined. Whereas the

Published OnlineFirst September 26, 2014; DOI: 10.1158/0008-5472.CAN-14-1106

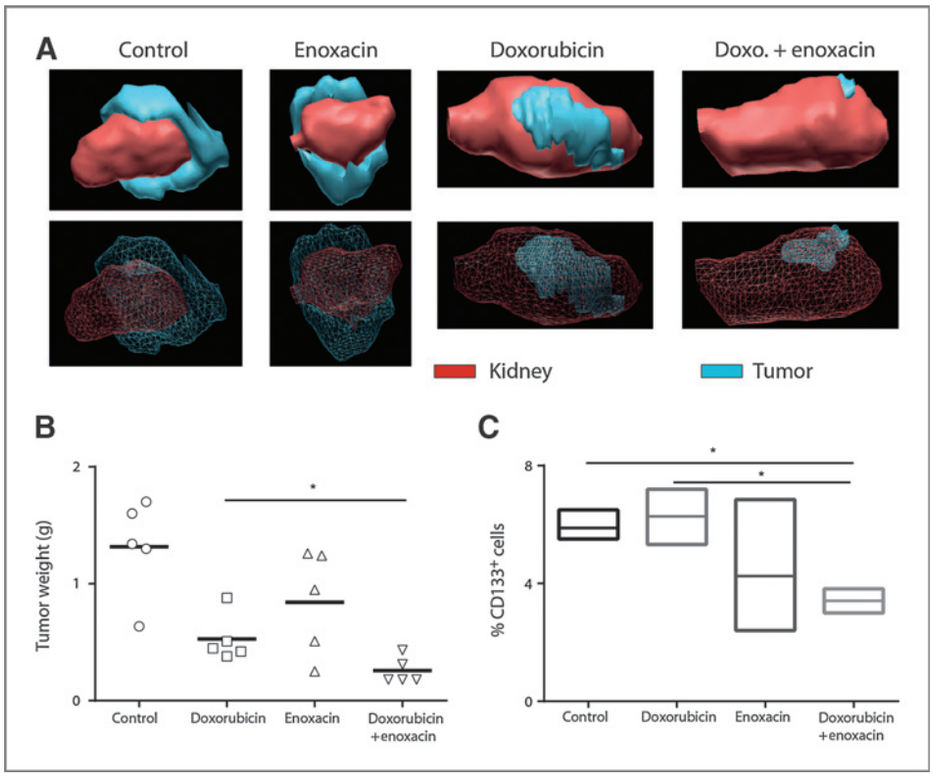

Figure 5. Synergistic antitumor activity of doxorubicin and enoxacin on primary ESFT xenografts. A, representative 3D reconstruction of ultrasound images of ESFT-3 tumors after 4 weeks of the indicated treatment. B, tumor weight of ESFT-3 after 5 weeks of treatment with vehicle, enoxacin alone (50 mg/kg 5 days/week), doxorubicin alone (single weekly 0.5 mg/kg dose), or a combination of the two drugs at the same doses. The Student *t* test was performed for comparison of doxorubicin only– and doxorubicin/enoxacin-treated groups. C, $CD133^+$ cell fraction in residual ESFT-3 following treatment. Results were analyzed by one-way ANOVA, and mean values with distribution are shown. *, $P < 0.05$.

volume of tumors derived from metastatic ESFT-3 cells was hardly affected by enoxacin alone and only mildly so by doxorubicin alone (Fig. 5A), combined doxorubicin–enoxacin treatment markedly decreased tumor volume, as assessed by ultrasonography 4 weeks following initiation of the treatment (Fig. 5A), without significantly affecting body weight. Accordingly, at autopsy, 7 days following the ultrasonography images shown in Fig. 5A, tumor weight was found to be mildly decreased by enoxacin alone, more markedly so by doxorubicin alone and strongly by the combination of the two drugs (Fig. 5B). Comparable differences in response were observed upon treatment of ESFT-1 xenografts (Supplementary Fig. S2A). Assessment of CD133 expression following treatment of ESFT-1 and ESFT-3 confirmed the observations made *in vitro*. The fraction of $CD133^+$ cells was unaltered in doxorubicin only–treated tumors, whereas enoxacin only–treated tumors had decreased $CD133^+$ cell counts (Fig. 5C). Combined treatment markedly depleted $CD133^+$ cells (Fig. 5C and Supplementary Fig. S2B).

Residual tumors following combined enoxacin–doxorubicin treatment display extensive necrosis, decreased numbers of $CD133^+$ cells, and restored miRNA expression

Residual tumors following each treatment regimen were subjected to histologic H&E analysis and, whenever possible, 200 mg of tumor tissue was dissociated for live-cell quantification and RNA extraction. Whereas control and doxorubicin only–treated tumors displayed limited necrosis, extensive necrosis was observed in tumors removed from enoxacin/doxorubicin-treated mice (Fig. 6A). Live-cell counts revealed a robust decrease in living ESFT-1 cells per gram of tumor, consistent with histologic findings (Fig. 6B).

To verify that the effect of enoxacin on primary ESFT did not reflect off-target effects, we assessed miRNA expression in residual tumors. Expression of a subset of TARBP2-dependent miRNAs was increased in combination-treated tumors compared with control or doxorubicin alone–treated tumors (Fig. 6C), consistent with the mechanism of action of enoxacin in restoring TARBP2-dependent miRNA maturation (19).

Serial transplantation of residual ESFT-1 cells from tumors having undergone combined treatment shows a decrease in tumor-initiating capacity

To assess whether combined enoxacin/doxorubicin treatment of ESFT xenografts eradicates tumor-initiating cells, 5,000 unsorted cells from treated xenografts were injected beneath kidney capsules of NSG recipient mice and allowed to engraft without any additional treatment. Whereas cells from all seven of seven control tumors and five of seven doxorubicin only–treated tumors developed new growth 8 weeks following serial xenotransplantation, cells from combination-treated tumors reinitiated tumor growth in only 3 of 7 mice (Fig. 6D). The $CD133^+$ population persisted in both control and residual tumors from doxorubicin only–treated mice and was either unchanged or increased in tumors that arose from serial xenotransplantation of these residual cells (Fig. 6E). In contrast, $CD133^+$ cells were strongly depleted or absent in residual tumors from mice that had received the combined enoxacin–doxorubicin treatment. However, in the

Published OnlineFirst September 26, 2014; DOI: 10.1158/0008-5472.CAN-14-1106

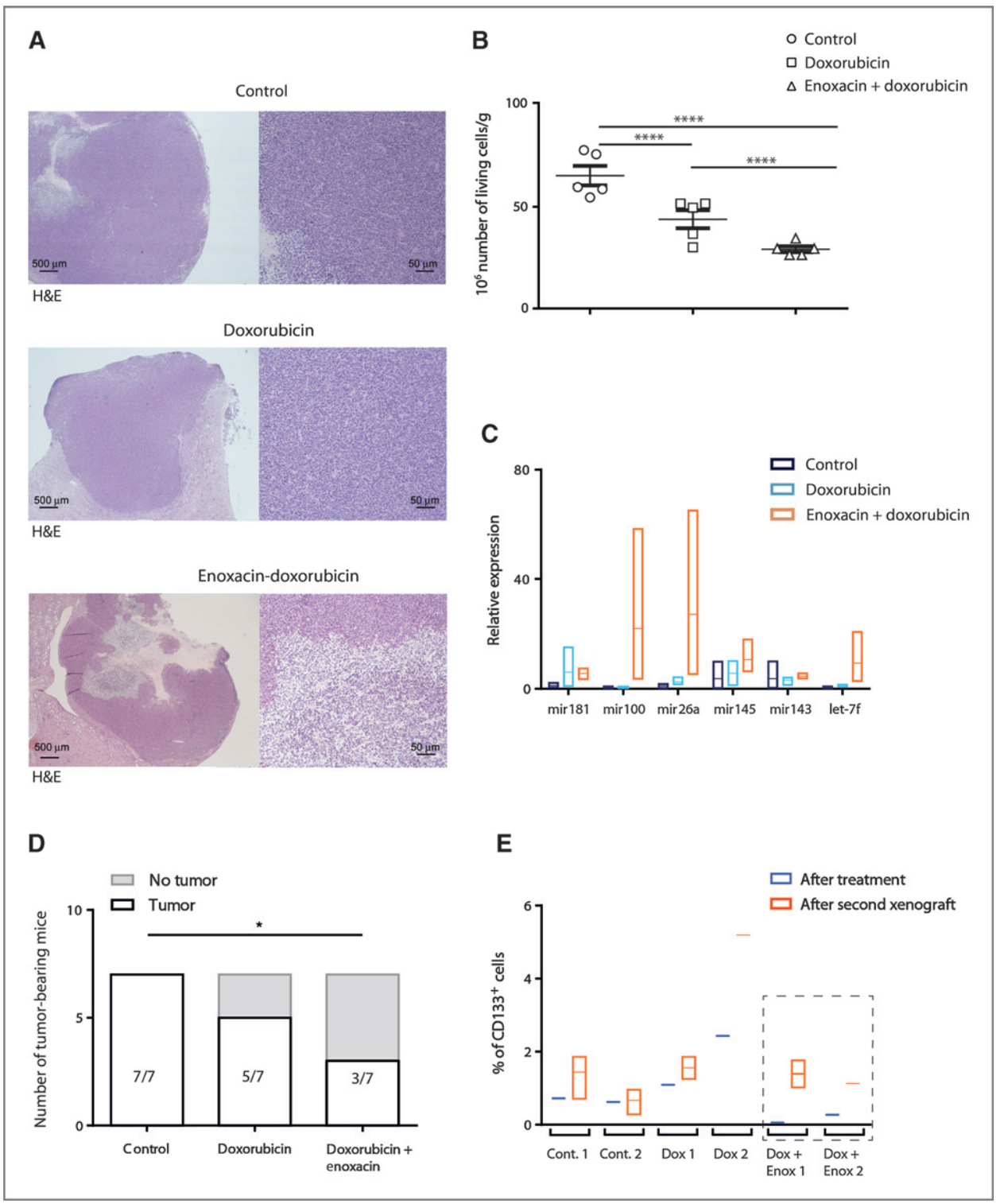

Figure 6. Enoxacin in combination with doxorubicin induces extensive tumor necrosis *in vivo*, increases miRNA expression, and depletes tumor-initiating capacity. A, H&E staining of residual tumors (ESFT-1) 5 weeks after the indicated treatment. B, number of living cells $\times$ 10^6/gram of dissociated tumor following treatment. Results were analyzed by one-way ANOVA. C, relative fold change of miRNA expression in residual tumors as assessed by RT-PCR. Mean values and distributions are shown. D, 5000 residual viable cells from treated tumors (ESFT-1) were reinjected into healthy recipient mice and tumor development was scored 6 weeks later. Data were analyzed by the χ^2 test. E, percentage of $CD133^+$ cells in residual tumors following treatment (before reinjection) and in secondary xenografts. Mean values and distribution are indicated. *, $P < 0.05$; ****, $P < 0.0001$.

Published OnlineFirst September 26, 2014; DOI: 10.1158/0008-5472.CAN-14-1106

three tumors that grew as a result of serial xenotransplants of cells from residual combination-treated tumors, CD133$^+$ cells reemerged and formed roughly 1% to 2% of the tumor bulk (Fig. 6E).

Identification of a candidate predictor of ESFT response to enoxacin that may also serve as a potential prognostic marker

Our observations suggest that ESFT patients who are likely to benefit from enoxacin treatment could be selected on the basis of their CSC miRNA profile. However, such an approach would be highly impractical. We therefore sought for a protein whose expression in ESFT cells, modulated by TARBP2-dependent miRNAs, may predict responsiveness to enoxacin. We first identified 111 common target genes of at least three of five TARBP2-dependent miRNAs, which are consistently downregulated in CSC, including let-7f, miRNA-145, miRNA-181a, miRNA-26a, and miRNA-100 (Supplementary Table S1). Assessment of the collective relevance of these common targets to ESFT pathogenesis was performed by clustering a cohort of 44 primary ESFT patients available from GEO under the accession number GSE17679 based on expression of the 111 genes and comparing the two clusters for survival. Clear separation in survival probability between the two clusters that fell just below statistical significance was observed (Fig. 7A). Assessment of the possible relationship between individual gene expression and patient survival in the 44 primary ESFT cohort revealed that at a 10% FDR, 37 of 111 probes significantly correlated with survival (Fig. 7A and B). Among them, onecut2, a miRNA-regulated homeobox protein implicated in hepatocyte (22) and neural differentiation (23), epithelial-to-mesenchymal transition (EMT), and colon cancer prognosis (24), appeared as a candidate prognostic marker. ESFT patients with onecut2 expression above and below the median value displayed significant difference in survival (Fig. 7C). Moreover, onecut2 expression in ESFT CD133$^+$ cells (Fig. 7D) and spheres (data not shown) correlated with responsiveness to enoxacin as assessed by clonogenicity and Annexin PI assays (Fig. 7D). Interestingly, the highest expressor of onecut2, ESFT2, also displayed the greatest difference in expression levels of TARBP2-dependent miRNAs between spheres and adherent cells. Thus, onecut2 may be a candidate predictor of response to enoxacin, pending validation in a large number of primary tumors.

Discussion

Our present observations support the notion that ESFT CSC and cells that constitute the ESFT bulk display distinct sensitivity to different therapeutic regimens. Thus, doxorubicin, an intercalating agent (25) that targets rapidly proliferating tumor cells and is currently the main agent of first line chemotherapy in ESFT treatment (11), had little effect *in vitro* on ESFT spheres, which are enriched in CSC, whereas it was significantly more toxic to adherent cells, which more closely recapitulate the tumor bulk. Conversely, enoxacin, which like other fluoroquinolones targets type II and type IV topoisomerases in Gram-negative and Gram-positive bacteria, respectively (19), but which in mammalian cells augments TARBP2 affinity for its substrate pre-miRNAs, leading to increased miRNA maturation (19), affected cells grown as spheres but spared adherent cells. In response to enoxacin, sphere-derived cells lost clonogenic properties and in two out of the four primary tumor samples, CD133$^+$ subpopulations underwent massive apoptosis.

Importantly, doxorubicin and enoxacin displayed a synergistic effect on primary ESFT xenotransplants *in vivo*. Doxorubicin alone had virtually no effect on ESFT-1 and only a moderate effect on ESFT-3 xenografts, but its effectiveness was markedly increased when combined with enoxacin. As a single agent, doxorubicin only mildly affected the CSC compartment, if at all, *in vivo*, as CD133$^+$ cell numbers in both ESFT-1 and ESFT-3 cells were comparable in control and doxorubicin-treated tumors. Furthermore, there was little difference in the initiation of tumor growth after secondary transplantation of cells from untreated or doxorubicin-treated tumors. Thus, whereas it eliminates a substantial portion of cells that constitute the tumor bulk, doxorubicin spares sufficient tumor-initiating cells to allow regrowth following cessation of treatment. In contrast, enoxacin depletes the CSC compartment, even at the relatively mild doses used to treat infection, but leaves rapidly dividing cells that form the tumor mass largely unscathed. Surprisingly, enoxacin only–treated tumors displayed focal necrosis and tumor cell dissociation, suggesting vascular and/or extracellular matrix (ECM) defects. ESFT cells can form vessel-like tubes *in vitro* and express genes associated with vasculogenic mimicry (26), possibly in relation to the function of FLI-1 as a major endothelial transcription factor (27). Similar to their glioblastoma counterparts (28), a fraction of ESFT CSCs may undergo vascular reprogramming and participate in tumor vascularisation. Their selective targeting may provide a possible explanation for the observed multifocal necrosis and changes in tumor architecture in response to enoxacin.

In combination, enoxacin and doxorubicin depleted the CD133$^+$ CSC compartment and induced massive cell death in the tumor bulk, leaving small, highly necrotic tumors. Moreover, xenografts from both a primary (ESFT-1) and a highly aggressive terminal phase tumor that had escaped all conventional therapeutic regimens (ESFT-3) responded to the combined treatment, suggesting that such a strategy may be of benefit even in late-stage disease, irrespective of lengthy prior exposure to chemotherapy. *In vitro* data suggest that the observed synergy between doxorubicin and enoxacin is not the result of cumulative drug toxicity (Supplementary Fig. S1C) but is primarily due to their targeting of different cell subpopulations. However, the markedly stronger inhibition of tumor growth by combined enoxacin–doxorubicin treatment compared with that of either drug alone suggests that in addition to targeting a distinct cell subpopulation, enoxacin may potentiate the cytotoxic effect of doxorubicin, possibly by targeting CSCs that undergo reprogramming toward vasculogenic mimicry leading to increased vascular permeability, which may facilitate doxorubicin delivery.

Consistent with the notion that enoxacin depletes CSC, cells from residual doxorubicin/enoxacin-treated tumors displayed

Published OnlineFirst September 26, 2014; DOI: 10.1158/0008-5472.CAN-14-1106

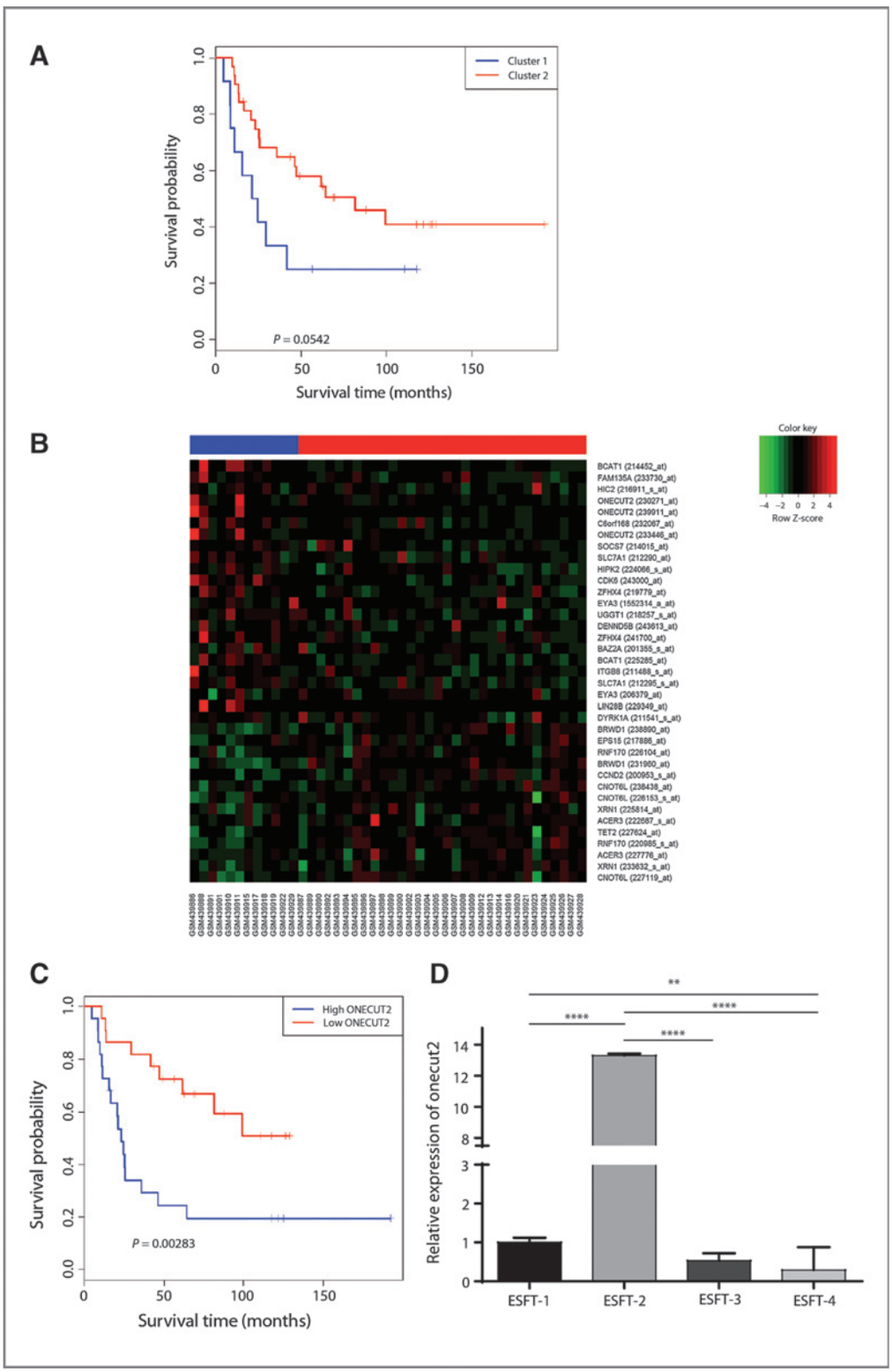

Figure 7. Onecut2, a candidate predictor marker of ESFT response to enoxacin whose expression may correlate with prognosis. A, Kaplan–Meier curve of the clustering of 111 targets of at least three out of five miRNAs (let-7f, mir-26a, mir-100, mir-145, and mir-181a). B, clustering of 37 individual significantly prognostic targets of three out of five miRNAs. C, Kaplan–Meier curve of survival probability of patients, according to *ONECUT2* expression above or below the median. D, expression of *ONECUT2* in the CD133^{+} fraction of the four ESFT samples relative to that of ESFT-1. Results analyzed by one-way ANOVA. Mean values ± SD are shown. **, $P < 0.01$; ****, $P < 0.0001$.

Published OnlineFirst September 26, 2014; DOI: 10.1158/0008-5472.CAN-14-1106

impaired tumor-initiating capacity compared with cells from control and doxorubicin only–treated tumors. Interestingly, the tumors that did form contained a $CD133^+$ cell subpopulation despite the fact that the injected cells had no detectable CD133 expression. Although we cannot formally exclude the presence of a few undetected $CD133^+$ cells in residual tumors following combined treatment that reconstituted the $CD133^+$ subpopulation, it is conceivable that $CD133^+$ cells in the secondary xenotransplants emerged as a result of reprogramming of nontumorigenic cells toward the CSC phenotype. Mounting evidence indicates that nontumorigenic cells may undergo such reprogramming, thereby resuming initiation of tumor growth even after seemingly effective CSC eradication (29). Maintenance of combined targeting of CSCs and the tumor bulk therefore seems recommended for the duration of the treatment.

The observations that defective TARBP2 function underlies ESFT CSC emergence and that fluoroquinolones enhance TARBP2 activity and corresponding miRNA maturation have led to the discovery of unpredicted synergy between enoxacin and standard-of care-chemotherapy toward controlling ESFT growth. As our understanding of mechanisms that are responsible for CSC emergence is still in its infancy, it is difficult to predict how broadly applicable to divergent tumor types such an approach may be. Nevertheless, our observations demonstrate that combining doxorubicin with enoxacin provides a rational, mechanism-based therapeutic approach in ESFT that successfully targets two key cell subpopulations.

Disclosure of Potential Conflicts of Interest

No potential conflicts of interest were disclosed.

Authors' Contributions

Conception and design: S. Cornaz-Buros, N. Riggi, C. DeVito, I. Stamenkovic
Development of methodology: S. Cornaz-Buros, N. Riggi, C. DeVito
Acquisition of data (provided animals, acquired and managed patients, provided facilities, etc.): S. Cornaz-Buros, N. Riggi, A. Sarre, I. Letovanec
Analysis and interpretation of data (e.g., statistical analysis, biostatistics, computational analysis): S. Cornaz-Buros, N. Riggi, A. Sarre, I. Letovanec, P. Provero, I. Stamenkovic
Writing, review, and/or revision of the manuscript: S. Cornaz-Buros, N. Riggi, C. DeVito, A. Sarre, I. Letovanec, I. Stamenkovic
Administrative, technical, or material support (i.e., reporting or organizing data, constructing databases): I. Letovanec
Study supervision: N. Riggi, I. Stamenkovic

Acknowledgments

The authors thank Giula Fregni, Emely Moller, and Patrick Rodriguez for critical review of the article.

Grant Support

This study was supported by an FNS grant 310030_150024, Oncosuisse Grant 2766-02-2011, and ISREC Foundation Sarcoma Grant (I. Stamenkovic); FNS grant 32360-133894 (S. Cornaz-Buros); FNS grant P3SMP3_148408 and Nuovo Soldati Foundation grant (N. Riggi).

The costs of publication of this article were defrayed in part by the payment of page charges. This article must therefore be hereby marked *advertisement* in accordance with 18 U.S.C. Section 1734 solely to indicate this fact.

Received April 17, 2014; revised August 20, 2014; accepted September 2, 2014; published OnlineFirst September 26, 2014.

References

1. Nowell PC. Tumor progression: a brief historical perspective. Semin Cancer Biol 2002;12:261–6.
2. Baylin SB, Jones PA. A decade of exploring the cancer epigenome - biological and translational implications. Nat Rev Cancer 2011;11:726–34.
3. Polyak K, Haviv I, Campbell IG. Co-evolution of tumor cells and their microenvironment. Trends Genet 2009;25:30–8.
4. Reya T, Morrison SJ, Clarke MF, Weissman IL. Stem cells, cancer, and cancer stem cells. Nature 2001;414:105–11.
5. Dick JE. Stem cell concepts renew cancer research. Blood 2008;112:4793–807.
6. Meacham CE, Morrison SJ. Tumour heterogeneity and cancer cell plasticity. Nature 2013;501:328–37.
7. Clevers H. The cancer stem cell: premises, promises and challenges. Nat Med 2011;17:313–9.
8. Bao S, Wu Q, McLendon RE, Hao Y, Shi Q, Hjelmeland AB, et al. Glioma stem cells promote radioresistance by preferential activation of the DNA damage response. Nature 2006;444:756–60.
9. Diehn M, Cho RW, Lobo NA, Kalisky T, Dorie MJ, Kulp AN, et al. Association of reactive oxygen species levels and radioresistance in cancer stem cells. Nature 2009;458:780–3.
10. Oravecz-Wilson KI, Philips ST, Yilmaz OH, Ames HM, Li L, Crawford BD, et al. Persistence of leukemia-initiating cells in a conditional knockin model of an imatinib-responsive myeloproliferative disorder. Cancer Cell 2009;16:137–48.
11. Potratz J, Dirksen U, Jurgens H, Craft A. Ewing sarcoma: clinical state-of-the-art. Pediatr Hematol Oncol 2012;29:1–11.
12. Suva ML, Riggi N, Stehle JC, Baumer K, Tercier S, Joseph JM, et al. Identification of cancer stem cells in Ewing's sarcoma. Cancer Res 2009;69:1776–81.
13. Riggi N, Stamenkovic I. The biology of ewing sarcoma. Cancer Lett 2007;254:1–10.
14. De Vito C, Riggi N, Cornaz S, Suva ML, Baumer K, Provero P, et al. A TARBP2-dependent miRNA expression profile underlies cancer stem cell properties and provides candidate therapeutic reagents in Ewing sarcoma. Cancer Cell 2012;21:807–21.
15. Krol J, Loedige I, Filipowicz W. The widespread regulation of microRNA biogenesis, function and decay. Nat Rev Genet 2010;11:597–610.
16. Croce CM. Causes and consequences of microRNA dysregulation in cancer. Nat Rev Genet 2009;10:704–14.
17. Riggi N, Suva ML, De Vito C, Provero P, Stehle JC, Baumer K, et al. EWS-FLI-1 modulates miRNA145 and SOX2 expression to initiate mesenchymal stem cell reprogramming toward Ewing sarcoma cancer stem cells. Genes Dev 2010;24:916–32.
18. Brohl AS, Solomon DA, Chang W, Wang J, Song Y, Sindiri S, et al. The genomic landscape of the Ewing Sarcoma family of tumors reveals recurrent STAG2 mutation. PLoS Genet 2014;10:e1004475.
19. Shan G, Li Y, Zhang J, Li W, Szulwach KE, Duan R, et al. A small molecule enhances RNA interference and promotes microRNA processing. Nat Biotech 2008;26:933–40.
20. Holohan C, Van Schaeybroeck S, Longley DB, Johnston PG. Cancer drug resistance: an evolving paradigm. Nat Rev Cancer 2013;13:714–26.
21. Wolf R, Eberl R, Dunky A, Mertz N, Chang T, Goulet JR, et al. The clinical pharmacokinetics and tolerance of enoxacin in healthy volunteers. J Antimicrob Chemother 1984;14:63–9.
22. Laudadio I, Manfroid I, Achouri Y, Schmidt D, Wilson MD, Cordi S, et al. A feedback loop between the liver-enriched transcription factor network and miR-122 controls hepatocyte differentiation. Gastroenterology 2012;142:119–29.
23. Francius C, Clotman F. Dynamic expression of the Onecut transcription factors HNF-6, OC-2 and OC-3 during spinal motor neuron development. Neuroscience 2010;165:116–29.

Published OnlineFirst September 26, 2014; DOI: 10.1158/0008-5472.CAN-14-1106

24. Sun Y, Shen S, Liu X, Tang H, Wang Z, Yu Z, et al. MiR-429 inhibits cells growth and invasion and regulates EMT-related marker genes by targeting Onecut2 in colorectal carcinoma. Mol Cell Biochem 2014;390:19–30.
25. Tacar O, Dass CR. Doxorubicin-induced death in tumour cells and cardiomyocytes: is autophagy the key to improving future clinical outcomes? J Pharm Pharmacol 2013;65:1577–89.
26. van der Schaft DW, Hillen F, Pauwels P, Kirschmann DA, Castermans K, Egbrink MG, et al. Tumor cell plasticity in Ewing sarcoma, an alternative circulatory system stimulated by hypoxia. Cancer Res 2005;65:11520–8.
27. Liu F, Walmsley M, Rodaway A, Patient R. Fli1 acts at the top of the transcriptional network driving blood and endothelial development. Curr Biol 2008;18:1234–40.
28. Wang R, Chadalavada K, Wilshire J, Kowalik U, Hovinga KE, Geber A, et al. Glioblastoma stem-like cells give rise to tumour endothelium. Nature 2010;468:829–33.
29. Magee JA, Piskounova E, Morrison SJ. Cancer stem cells: impact, heterogeneity, and uncertainty. Cancer Cell 2012;21:283–96.

Cancer Research
The Journal of Cancer Research (1916–1930) | The American Journal of Cancer (1931–1940)

AACR American Association for Cancer Research

Targeting Cancer Stem–like Cells as an Approach to Defeating Cellular Heterogeneity in Ewing Sarcoma

Sandrine Cornaz-Buros, Nicolo Riggi, Claudio DeVito, et al.

Cancer Res 2014;74:6610-6622. Published OnlineFirst September 26, 2014.